Revista Brasileira de Ciência do Solo

Division – Soil Processes and Properties | Commission – Soil Physics

A novel approach based on X-ray fluorescence and photon attenuation to the analysis of soils for forensic investigation

Luiz Fernando Pires[(1)]* (iD), **Luis Valério Prandel**[(1)] (iD), **Sérgio da Costa Saab**[(1)] (iD) and **André Maurício Brinatti**[(1)] (iD)

[(1)] Universidade Estadual de Ponta Grossa, Departamento de Física, Ponta Grossa, Paraná, Brasil.

* Corresponding author:
E-mail: lfpires@uepg.br

ABSTRACT: Use of soil in forensic science is related to its several chemical, physical, and biological properties associated with its capacity to adhere to different materials and surfaces. Forensic soil experts and police investigators have been using soil samples as an aid in criminal investigations. Soils can act as fingerprints because they present contrasting physical, chemical, biological, and mineralogical properties. However, depending on the analytical tools utilized to characterize the soil, differentiating the samples when they have similar properties might be impossible. Thus, soil utilization as a fingerprint material requires increasing the number of variables measured as well as the accuracy and precision of the measurements. This study presents the feasibility of methods based on X-ray fluorescence (XRF) and radiation interaction parameters to discriminate soils for forensic investigations. Analyses of soil particle size, elemental composition (XRF), mass attenuation coefficient (μ), atomic (σ_a) and electronic (σ_e) cross-sections, effective atomic number (Z_{eff}), and electron density (N_{el}) were carried out to evaluate the potential of nuclear parameters to differentiate soils. Ten different soil types collected at 0.00-0.05 m layer were studied. The radiation interaction parameters were obtained through the XCOM computer code, while the experimental measurements were carried out by the traditional gamma-ray attenuation method utilizing the radioactive sources of ^{241}Am and ^{137}Cs. The results showed that the soils presented broad differences in terms of clay, silt, and sand contents as well as in the major oxides. These differences influenced the radiation attenuation properties as verified through the multivariate analysis. For the lowest photon energy studied (10 and 30 keV), σ_e was the most interesting parameter to discriminate the soils. For energies above 59.5 keV, Z_{eff} and N_{el} were the most important parameters. Good agreement was found between the calculated and measured parameters. The findings of this study indicate that radiation interaction parameters have great potential for crime scene investigation providing new parameters for better discrimination of soils. The main advantage of the method presented here is that it is fast, easy to implement, does not require powerful computers, and the XCOM code can be run online at the NIST (National Institute of Standards and Technology, USA) website.

Keywords: atomic cross-section, effective atomic number, electronic cross-section, mass attenuation coefficient, XCOM.

INTRODUCTION

Soils are complex systems that present different chemical, physical, and mineralogical properties. The distinct compositions of the solid phase in the soil related to texture, mineralogy, oxide types, organic matter contents, etc., make this material suitable for forensic purposes (Kammrath et al., 2018; Melo et al., 2020; Testoni et al., 2020). Soil analyses applied to forensic sciences are usually based on color, texture, particle size distribution, mineral identification, etc. (Prandel et al., 2018; Testoni et al., 2019). Most of the current analytical methods employed present the advantages of not destroying the samples, being reliable, sensitive, and not requiring large amounts of material for the analyses (Kammrath et al., 2018; Prandel et al., 2019; Melo et al., 2020).

The techniques utilized for soil analysis for forensic investigations include, for example, tools such as morphologically-directed Raman spectroscopy. This technique combines particle analysis with Raman spectroscopy that can be employed to probe the molecular chemistry of specific particles of interest (Kammrath et al., 2018). Scanning electron microscopy and energy dispersive X-ray spectrometry are other quantitative methods usually used to analyze soils (Bergslien, 2013; Nakai et al., 2013; Woods et al., 2014; Uitdehaag et al., 2017; Prandel et al., 2019; Melo et al., 2020). These methods allow the investigator to map particles in terms of their mineralogy (Kikkawa et al., 2019). Soil mineral analysis through X-ray diffraction is another commonly employed technique due to its capability to obtain mineralogical composition, crystallite size, atomic positions, etc. (Gonçalves et al., 2008; Prandel et al., 2018).

Furthermore, traditional methods of soil analysis have also been used to measure organic matter content, pH, particle-size distribution, particle density, among other properties (Bonetti and Quarino, 2014). These conventional methods are usually easy-to-use and cost-effective in relation to other more modern analytical tools. Nonetheless, different soils may present similar physical and chemical properties. This means that the use of a single technique or a few of them for analyzing soils might not be enough to identify differences among them (Cheshire et al., 2017; Prandel et al., 2017).

Computer-based simulations of radiation interaction with matter can be easily carried out through tools such as Monte Carlo simulations and methods based on the mixture rule (XCOM) (Berger and Hubbel, 1987; Pires, 2018). If the soil characteristics are analyzed adequately through a combination of traditional methods (e.g., particle size analysis) and more modern ones (e.g., X-ray fluorescence (XRF), X-Ray microtomography, atomic force microscopy); and supposing that no differences are observed in the results obtained from different soils, the use of other parameters based on those previously measured (e.g., soil oxides) can be an interesting alternative to discriminate soils encountered in crime scenes (Medhat et al., 2014; Pires et al., 2016).

Radiation interaction properties such as mass attenuation coefficient (μ), atomic (σ_a) and electronic (σ_e) cross-sections, effective atomic number (Z_{eff}), and electron density (N_{el}) can be determined when the composition and density of the materials are known (Han and Demir, 2009; Medhat and Pires, 2016; Ferreira et al., 2018). Many types of analyses can be conducted based on these parameters and XRF measurements, such as variations of the interaction parameters with photon energy or the contribution of processes such as the photoelectric effect, coherent and incoherent scatterings, and pair production to the mass attenuation coefficient (Camargo et al., 2021).

In this study, the main interest is to present a new methodology to the forensic soil science field, which allows an increase in the number of parameters evaluated for better discrimination among soils. Thus, this study aims to present radiation interaction parameters as fingerprints to discriminate soils. Our main hypothesis is that properties based on radiation attenuation might be employed to characterize soils for forensic applications. To obtain the radiation parameters, the studied soils were first submitted

to elemental analysis through energy dispersive X-ray fluorescence. After that, the XCOM computer code computed the total and partial mass attenuation coefficients, which were further employed to calculate σ_a, σ_e, Z_{eff} and N_{el}.

MATERIALS AND METHODS

For this study, soil samples derived from ten sample sites were chosen and sampled in different regions of the Paraná State, Brazil (Figure 1). The disturbed samples were collected at 0.00-0.05 m layer using stainless flat bottom scoops, stainless spatulas, and gloves to minimize soil contamination. All the samples were placed in clean plastic bags for further laboratory analyses. Only samples from the soil surface were selected because soil evidence to be found on shoe soles, for example, is more probable to belong to the topsoil. The soil samples were identified, according to the sites where they were collected, as: PTB: Pato Bragado; PGC: Ponta Grossa; STH: Santa Helena; MER: Mercedes; MOR: Morretes; RAZ: Rio Azul; LAP: Lapa; CAZ: Cerro Azul; JOT: Joaquim Távora; and PAR: Paranavaí (Table 1). The areas selected for sampling were close to urban zones located near international and state borders, international harbor, and metropolitan regions (Figure 1).

The soil texture was determined using the pipette method (Gee and Bauder, 1986). Samples of air-dried and sieved (2 mm aperture sieve) soils were dispersed using 10 mL NaOH (1 mol L^{-1}) per 100 mL water and ultrasonic treatment (Vibra-Cell equipment, by Sonics), at 20 W for 5 min, and manual stirring (1 min) was performed to facilitate soil dispersion. After these initial procedures, the soil sample solution was kept at rest for 24 h. The samples were prepared in triplicate through the sedimentation method using the Stokes law (Tanner and Jackson, 1948; Prandel et al., 2017). The USDA textural soil classification system was utilized to classify the soil samples (United States Department of Agriculture, 1987) (Table 1).

Soil particle density measurement was carried out using the pycnometer method (Blake and Hartge, 1986). Clean and dry pycnometers were employed in all the measurements. Around 300 mg of sieved (2 mm aperture sieve) and powdered (using agate crucible and pestle) dry soil was put in the pycnometers; distilled and de-aired water was used to fill them in a temperature-controlled environment. An accurate balance (Gehara AG200, 10^{-4} g accuracy) was employed in all the measurement procedures. Three measurements were carried out for each soil.
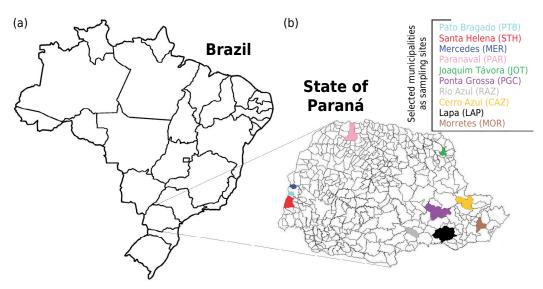

Figure 1. Map of Brazil locating the state of Paraná (a) and the municipalities' location (b) where the soil samples were collected.

Semi-quantitative elemental analysis of the whole soils was accomplished using the energy dispersive X-ray fluorescence technique (XRF) with the instrument model EDX-720 (Shimadzu) equipped with an Rh X-ray tube. The equipment voltage varied from 5 to 50 kV and its tube current from 1 to 1000 µA. The system detector was a Si(Li) semi-conductor cooled with liquid N at -196 °C. Before the XRF analysis, the soil samples were dried (forced air oven set at 45 °C) and ground using agate crucible and pestle, until a uniform powder was obtained. The powdered and sieved (53 µm aperture sieve) sample portion (2 g) was placed into a sample analysis cup (supplied by the equipment manufacturer – around 22 mm diameter) for measurements. The soil thickness in the sample analysis cup was around 4 mm. The sample cup was covered with Mylar film (6 µm thick) for analysis. Each sample was measured for 100 s in the energy region of Na-Sc with a 15 kV voltage and in the energy region of Ti-U with a 50 kV voltage. Measurements were performed under 30 Pa pressure. The following calibration standards supplied by the equipment manufacturer were utilized: A-720 (calibration) and SUS (reference material). Three measurements were made for each soil.

The Z_{eff}, N_{el}, σ_a and σ_e were obtained based on the soil oxide composition (Table 2) using the XCOM computer code (Berger and Hubbel, 1987). The XCOM software, NIST-database service (National Institute of Standards and Technology, 2016), was selected due to its user-friendliness and for being able to provide total mass attenuation coefficient (μ_T) as well as partial mass attenuation coefficients due to the photoelectric effect (μ_{Ph}),

Table 1. Information of the soil samples studied

Sample	Location	Coordinates	Texture
PTB	Pato Bragado	24° 62' S, 54° 23' W	Clay
PGC	Ponta Grossa	25° 09' S, 50° 09' W	Clay
STH	Santa Helena	24° 85' S, 54° 34' W	Clay
MER	Mercedes	24° 74' S, 53° 75' W	Clay
MOR	Morretes	25° 47' S, 48° 83' W	Clay loam
RAZ	Rio Azul	25° 75' S, 50° 68' W	Clay loam
LAP	Lapa	25° 78' S, 49° 72' W	Sandy clay loam
CAZ	Cerro Azul	24° 82' S, 49° 26' W	Silt loam
JOT	Joaquim Távora	23° 49' S, 49° 93' W	Sandy loam
PAR	Paranavaí	23° 08' S, 52° 49' W	Sand

Table 2. Oxide content (most commonly found in all samples) of different soils studied

Sample	Oxides					
	SiO_2	Al_2O_3	Fe_2O_3	SO_3	TiO_2	MnO
	×100 (%)					
PTB	0.3068	0.3542	0.2752	0.0104	0.0430	0.0033
PGC	0.2946	0.5204	0.1435	0.0102	0.0213	0.0004
STH	0.3186	0.3175	0.2891	0.0118	0.0461	0.0047
MER	0.3387	0.2965	0.2878	0.0124	0.0476	0.0061
MOR	0.5868	0.2445	0.1197	0.0145	0.0321	0.0009
RAZ	0.6842	0.2210	0.0483	0.0145	0.0083	0.0010
LAP	0.7144	0.2007	0.0444	0.0132	0.0103	0.0007
CAZ	0.7464	0.1604	0.0427	0.0142	0.0116	0.0014
JOT	0.7151	0.2106	0.0301	0.0125	0.0084	0.0005
PAR	0.7663	0.1847	0.0276	0.0140	0.0070	0.0003

coherent (μ_{Coh}) and incoherent scatterings (μ_{Incoh}), and pair production (μ_{PP}) in the field of the atomic nucleus and electrons (Kaplan, 1963).

For the evaluation of the radiation interaction parameters, the mass attenuation coefficient was firstly employed, and then the molecular, atomic, and electronic cross-sections were calculated (Equations 1 to 3) (Manohara et al., 2008; Han and Demir, 2010; Pires, 2018; Taqi et al., 2021). When radiation interacts with any material, the amount of attenuation is dependent on that material chemical composition, thickness, density, and photon energy. The mass attenuation coefficient represents a measure of the material ability to scatter or absorb the radiation per unit of mass. It is given by the ratio of the linear attenuation coefficient and the material density, and it usually does not depend on the physical state of the material, unlike the linear attenuation coefficient, which indicates the probability of a photon being scattered or absorbed per unit thickness of the absorber material (Kaplan, 1963; Han and Demir, 2010). Cross-section is another useful concept in radiation physics, which represents the probability that photons interact with matter through particular processes. In other words, it is a measure of the chance of photon collision (Kaplan, 1963; Manohara et al., 2008).

$$\sigma_M = \mu \left(\frac{M}{N_A} \right) \qquad \text{Eq. 1}$$

$$\sigma_A = \frac{\sigma_M}{\sum_i n_i} \qquad \text{Eq. 2}$$

$$\sigma_E = \frac{1}{N_A} \sum \frac{f_i A_i}{Z_i} (\mu)_i \qquad \text{Eq. 3}$$

in which: μ is the mass attenuation coefficient; N_A is the Avogadro's number; $M = \sum_i n_i A_i$ is the molecular weight of the compound; A_i is the molecular weight of the *ith* element; n_i is the number of formula unit of the molecule; $\sum_i n_i$ is the total number of formula unit of the compound; $f_i = \frac{n_i}{\sum_i n_i}$ and Z_i are the fractional abundance and the atomic number of the *ith* constituent element; and n_j is the number of atoms of the constituent element and $\sum_j n_j$ the total number of atoms present in the molecular formula.

The effective atomic number and the electron density were obtained through equations 4 and 5. When radiation interacts with heterogeneous materials such as soils, the photon interaction turns impossible to represent the atomic number uniquely (single number as in the case of an element) for these composite materials. Thus, the effective atomic number is defined when composite substances are studied. The other important parameter, the electron density, is defined as the number of electrons per unit mass of the absorber material (Manohara et al., 2008; Akkurt, 2011; Mann et al., 2015; Taqi et al., 2021).

$$Z_{eff} = \frac{\sigma_A}{\sigma_E} \qquad \text{Eq. 4}$$

$$N_{el} = \frac{\mu}{\sigma_E} = \left(\frac{Z_{eff}}{M} \right) N_A \sum_i n_i \qquad \text{Eq. 5}$$

In this study, photon energies of 10, 30, 59.5, 356, 661.6 and 1330 keV were selected for the theoretical analysis of the radiation interaction with the matter. The last four energies were selected due to their use in experimental measurements of μ through the ^{241}Am, ^{133}Ba, ^{137}Cs and ^{60}Co radioactive sources. A flowchart of the procedures carried out to calculate the soil radiation interaction parameters is presented in figure 2.

The experimental soil μ was determined using the ^{241}Am and ^{137}Cs radioactive sources having activities of 3.7 GBq (^{241}Am) and 7.4 GBq (^{137}Cs), respectively. The former emits monoenergetic photons of 59.5 keV while the latter releases photons of 661.6 keV. The detector utilized was a 7.62 × 7.62 cm NaI(Tl) scintillation crystal (ORTEC 905-4) coupled to a photomultiplier tube (Figure 3). Circular lead collimators of 2 mm diameter were

adjusted in front of the radioactive sources. Another collimator with 4.5 mm diameter was adjusted in front of the detector. Both collimators were adjusted and aligned (laser point) between the source and the detector. The radioactive source and detector were mounted 22 cm apart from one another. Details about the experimental procedures can be found in Pires (2018).
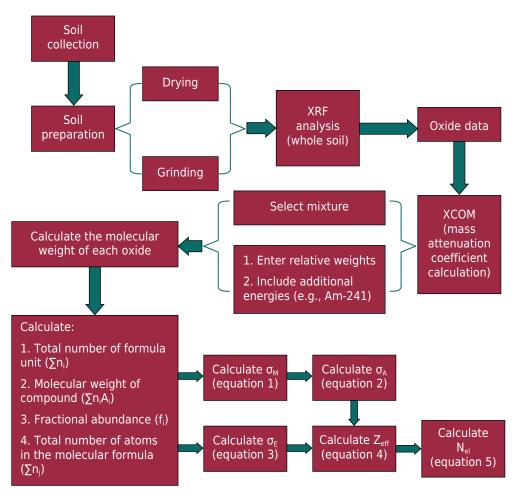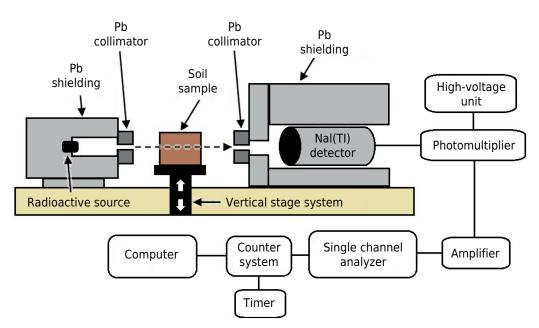
Figure 2. Flowchart of the procedures utilized for calculating the soil radiation interaction parameters.

Figure 3. Scheme of the gamma-ray attenuation system.

For the experimental evaluation of the soil attenuation coefficients, air-dried soil (105 °C for 24 h) samples were passed through a 2.0 mm sieve and packed into a thin wall (0.5 cm) acrylic container (0.10 × 0.10 × 0.10 m). The intensities (I) of the gamma-ray beam were measured in three different positions (vertical stage system) of the soil into the container. The value of the linear attenuation coefficient was obtained for each position, and after that, a mean value was calculated for each soil sample. A 600 s counting time was set for each measurement to obtain very good statistics (uncertainty <0.5 %). The linear attenuation coefficient was further converted in μ using the following equations:

$$\kappa = \frac{1}{x} \ln\left(\frac{I_0}{I}\right) \rightarrow \mu = \frac{\kappa}{\rho} \therefore \mu = \frac{1}{\rho x} \ln\left(\frac{I_0}{I}\right) \qquad \text{Eq. 6}$$

in which: I_0 is the incident photon intensity (no sample); I is the intensity after transmission through the sample of thickness x; and κ represents the linear attenuation coefficient. The soil bulk density (ρ) of the samples was obtained by the relation between the dry soil mass and the internal volume of the acrylic container filled with soil. As previously mentioned, the mass attenuation coefficient was calculated by the ratio between the linear attenuation coefficient of the absorber and its density (Equation 6).

The variables related to the textural and elemental analyses, as well as Z_{eff}, N_{el}, σ_a and σ_e (theoretical) of the whole soil samples and their fractions were exported to a data matrix and correlated using the Principal Component Analysis (PCA). Only the parameters with the greatest influence in the radiation attenuation were considered in the PCA analysis. The raw data were auto scaled before calculation. The PCA was performed using the Pirouette 4.5 software (Infometrix, USA). The sample scores were represented by the coordinate of the first principal component (PC-1) and second principal component (PC-2) linearly dependent on their respective variables and represented by the loading axes.

RESULTS

The soils studied showed textures varying from clay to sand (Table 1; Figures 4a and 4c). The amount of clay found presented a distribution between 8 (PAR) and 62 % (PTB); silt between 1 (PAR) and 56 % (CAZ); and sand between 17 (PGC) and 91 % (PAR) (Figure 4a). The particle density obtained varied from 2.41 (RAZ) to 2.72 Mg m^{-3} (STH) (Table 3). This property is closely related to the soil composition and the contribution of its fractions (Hillel, 2004; Lal and Shukla, 2004). The wide distribution of textures and particle densities analyzed highlights the importance of different particle sizes for radiation attenuation (Medhat and Pires, 2016; Ferreira et al., 2018). According to the USDA classification system, the sand fraction contains particles ranging in diameter from 2,000 to 50 μm, the silt fraction from 50 to 2 μm, and the clay fraction consists of <2 μm particles (Hillel, 2004).

Regarding the oxide content in each soil, SiO_2 ranged from c. 29.5 (PGC) to c. 76.6 % (PAR), Al_2O_3 from c. 16 (CAZ) to c. 52 % (PGC), and Fe_2O_3 from c. 2.8 (PAR) to c. 28.9 % (STH) (Table 2; Figure 4b). According to many published studies, tropical soils have a chemical composition comprised of major (SiO_2, Al_2O_3 and Fe_2O_3) and minor (CaO, K_2O, TiO_2, MnO, etc.) compounds (Sposito, 2008). In this study, the XRF analysis showed that SiO_2, Al_2O_3 and Fe_2O_3 (Table 2) contributed to over 92 % of the chemical composition of the soils studied as observed by other authors in Brazilian soils (Medhat et al., 2014; Pires et al., 2016; Ferreira et al., 2018; Camargo et al., 2021; Prandel et al., 2021).

The different photon energies analyzed in this study aimed to investigate the best energy to be used as tracing for forensic purposes. Energy values from 10 to 1330 keV were explored (Figures 5a to 5f). The radiation interaction parameters for specific energies of the [241]Am (59.5 keV), [133]Ba (356 keV), [137]Cs (661.6 keV) and [60]Co (1330 keV) radioactive sources were also investigated as these sources are usually employed in soil radiation interaction studies (Kucuk et al., 2013; Taqi et al., 2016).
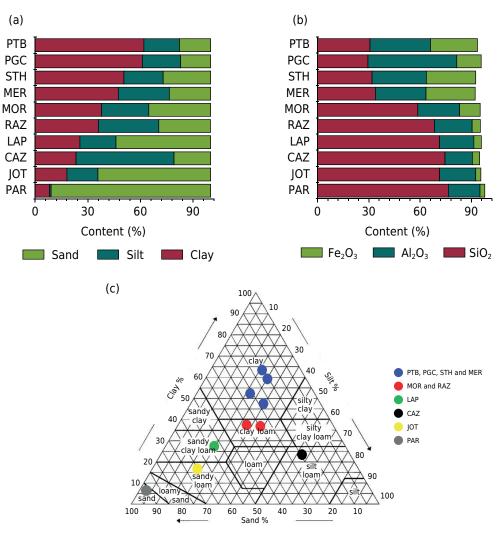
Figure 4. Sand, silt, and clay contents (a), Fe_2O_3, Al_2O_3, and SiO_2 contents (b), and the distribution of soil types based on percent sand, silt, and clay in the USDA texture triangle classification system (c). The acronyms utilized stand for the following municipalities: PTB (Pato Bragado), PGC (Ponta Grossa), STH (Santa Helena), MER (Mercedes), MOR (Morretes), RAZ (Rio Azul), LAP (Lapa), CAZ (Cerro Azul), JOT (Joaquim Távora), and PAR (Paranavaí).

Table 3. Total mass attenuation coefficient (μ_T) for the ^{241}Am and ^{137}Cs radioactive sources and particle density (PD) of the samples studied

Sample	μ_T				PD
	59.5 keV		661.6 keV		
	Meas.	Th.	Meas.	Th.	
	$cm^2\ g^{-1}$				$Mg\ m^{-3}$
PTB	0.434	0.450	0.0772	0.0759	2.52
PGC	0.320	0.353	0.0742	0.0761	2.50
STH	0.463	0.464	0.0751	0.0759	2.72
MER	0.468	0.493	0.0766	0.0760	2.53
MOR	0.315	0.344	0.0768	0.0765	2.50
RAZ	0.285	0.298	0.0728	0.0766	2.41
LAP	0.279	0.290	0.0771	0.0768	2.55
CAZ	0.275	0.292	0.0773	0.0769	2.57
JOT	0.275	0.281	0.0779	0.0769	2.53
PAR	0.260	0.277	0.0781	0.0769	2.59

Meas. and Th. stand for the measured and theoretical (calculated) values.

Regarding the small photon energies selected (10 and 30 keV), distinctions were noticed in the radiation interaction according to differences in the texture as well as the chemical compositions of the soils (Figures 5a to 5f). Concerning the lowest photon energy (10 keV), the parameter σ_e was greatly influenced by differences in the elemental composition of the soils (Figure 5a). This parameter varied from 74 (PAR) to 181 barn electron^{-1} (STH and MER). Santa Helena and Mercedes had almost the same amounts of clay, silt, sand, and similar contents of Fe_2O_3, while PAR had the smallest amount of Fe_2O_3 and the largest amount of sand (Figures 4a and 4b). These results show that σ_e is an interesting parameter
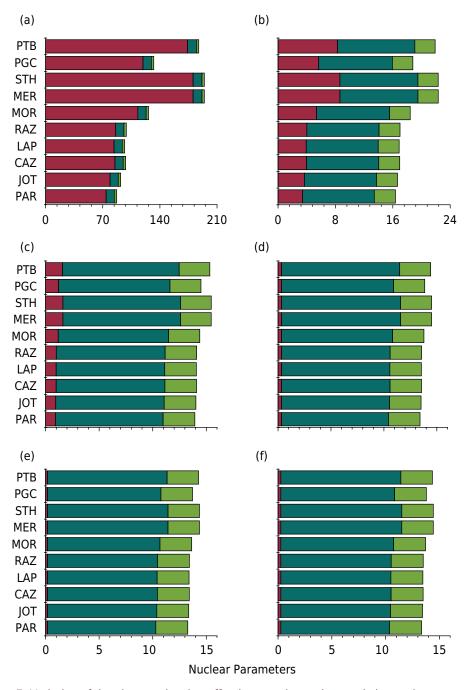

Figure 5. Variation of the electron density, effective atomic number, and electronic cross-section with photon energy. N_{el} (■), Z_{eff} (■), σ_e (■) at 10 keV (photon energy) (a), N_{el} (■), Z_{eff} (■), σ_e (■) at 30 keV (b), N_{el} (■), Z_{eff} (■), σ_e (■) at 59.5 keV (c), N_{el} (■), Z_{eff} (■), σ_e (■) at 356 keV (d), N_{el} (■), Z_{eff} (■), σ_e (■) at 661.6 keV (e), and N_{el} (■), Z_{eff} (■), σ_e (■) at 1330 keV (f). The acronyms utilized stand for the following municipalities: PTB (Pato Bragado), PGC (Ponta Grossa), STH (Santa Helena), MER (Mercedes), MOR (Morretes), RAZ (Rio Azul), LAP (Lapa), CAZ (Cerro Azul), JOT (Joaquim Távora), and PAR (Paranavaí). N_{el}: electron density, Z_{eff}: effective atomic number, σ_e: electronic cross-section.

to analyze radiation interaction, whereas Z_{eff} and N_{el} did not present differences among soils (Figure 5a). For the photon energy of 30 keV, σ_e and Z_{eff} showed the most important influences of the soil properties in the radiation interaction (Figure 5b). The parameter σ_e presented similarities with the results found for 10 keV, with variations between 3.4 (PAR) and 8.6 barn electron^{-1} (STH and MER). The Z_{eff} variations observed ranged from 9.99 (PAR) to 10.87 (STH and MER) (Figure 5b).

The increase in the photon energy (>50 keV) decreased the importance of σ_e to discriminate soils (Figures 5c to 5f). The parameters Z_{eff} and N_{el} presented almost the same tendencies among soils for all the remaining photon energies studied. With increased photon energy, the presence of elements of high Z tends to influence the values of Z_{eff} and N_{el} more significantly. Paranavaí was the soil with the smallest Z_{eff} for this interval of photon energies with values ranging from 10.05 (59.5 keV) to 10.11 (1330 keV), a difference of less than 1 % for an energy difference of around 22 times. On the other hand, STH and MER were the soils with the highest Z_{eff}, with values ranging from 10.98 (59.5 keV) to 11.25 (1330 keV).
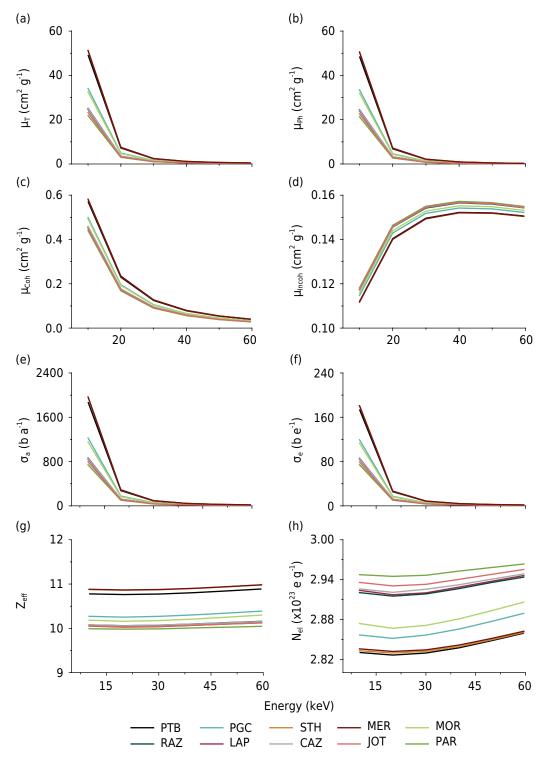
Regarding N_{el}, the lowest values in the energy range from 59.5 to 1330 keV were found for STH and MER (2.86×10^{-23} electrons g^{-1} for 59.5 keV and 2.93×10^{-23} electrons g^{-1} for 1330 keV), respectively (Figures 5c to 5f). A difference of around 2.5 % was observed for N_{el} between these two energies. The highest N_{el} was found in PAR (2.96×10^{-23} electrons g^{-1} for 59.5 keV and 2.98×10^{-23} electrons g^{-1} for 1330 keV). Thus, the Z_{eff} and N_{el} findings indicate that the use of sources with energies >50 keV produces almost the same type of results regardless of increases in photon energy (Figures 5c to 5f).
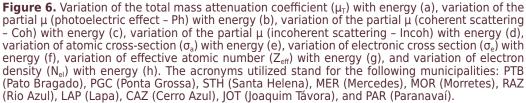
The total mass attenuation coefficient presented decreases increasing the photon energy as expected (Figure 6a). The highest μ_T values (theoretical) were found in STH and MER for all photon energies varying from 51.2 (10 keV) to 0.464 cm^2 g^{-1} (59.5 keV), whereas the lowest ones were observed in PAR (21.9 cm^2 g^{-1} for 10 keV and 0.277 cm^2 g^{-1} for 59.5 keV). These results of the μ_T variation as a function of photon energy agree with other studies for tropical/subtropical soils (Medhat et al., 2014; Pires et al., 2014). As seen in table 3, good agreement was observed between the measured and calculated values (XCOM) of μ_T for the ^{241}Am and ^{137}Cs radioactive sources. Relative differences between methods varied from 0.2 (STH) to 10.5 % (PGC), which is considered acceptable considering the errors associated with the experimental methods and the characteristics of the samples studied (Pires, 2018).

Regarding possible sources of errors, these are mainly related to counting statistics, nonuniformity of the sample measured, the presence of sample impurities, and scattered photons reaching the detector (dependent mainly on collimator size) (Luo and Wells, 1992). The semi-quantitative evaluation of the soil chemical composition through the XRF method can also be a source of error (theoretical measurements). The mixture rule used to give the mass attenuation coefficient is also prone to drawbacks because it disregards interactions among the atoms of the compounds (Almeida Junior et al., 2017). However, the comparison between the measured and calculated values indicates the reliability of the mass attenuation computer-based method to predict soil radiation interaction parameters, as already ratified by several studies (Cesareo et al., 1994; Akkurt et al., 2005; Manohara et al., 2008; Han and Demir, 2010; Kucuk et al., 2013; Medhat et al., 2014; Ferreira et al., 2018; Camargo et al., 2021; Taqi et al., 2021).

The partial mass attenuation coefficients due to the photoelectric effect and coherent scattering also presented the same behavior as observed for μ_T for the lowest photon energies (<50 keV) (Figures 6b and 6c). These results show the great influence of these two processes in the photon attenuation by the soils investigated. However, it seems relevant to highlight that the influence of the coherent scattering in μ_T is negligible when compared to the photoelectric effect (see the graph scales). In STH and MER, the μ_{Ph} contribution to the energies of 10 and 59.5 keV was 50.5 and 0.273 cm^2 g^{-1}, respectively (Figure 6b). For the lowest energy studied (10 keV), μ_{Ph} contributed with 99 % of the

total mass attenuation coefficient, while for 59.5 keV this contribution was around 60 %. According to Kaplan (1963), the photoelectric effect is the dominant process for low photon energies turning it the major contributor to μ_T. Incoherent scattering showed slight differences among soils for the energy range from 10 to 59.5 keV, with variations

Figure 6. Variation of the total mass attenuation coefficient (μ_T) with energy (a), variation of the partial μ (photoelectric effect – Ph) with energy (b), variation of the partial μ (coherent scattering – Coh) with energy (c), variation of the partial μ (incoherent scattering – Incoh) with energy (d), variation of atomic cross-section (σ_a) with energy (e), variation of electronic cross section (σ_e) with energy (f), variation of effective atomic number (Z_{eff}) with energy (g), and variation of electron density (N_{el}) with energy (h). The acronyms utilized stand for the following municipalities: PTB (Pato Bragado), PGC (Ponta Grossa), STH (Santa Helena), MER (Mercedes), MOR (Morretes), RAZ (Rio Azul), LAP (Lapa), CAZ (Cerro Azul), JOT (Joaquim Távora), and PAR (Paranavaí).

ranging from 0.151 (PTB, STH and MER) to 0.155 $cm^2 g^{-1}$ (PAR) for the latter (Figure 6d). This result indicates μ_{Incoh} contributions of 57 (PAR) and 33 % (PTB, STH and MER) to μ_T.

The atomic and electronic cross-sections also presented interesting results to discriminate the soils studied, especially for the lowest photon energies (Figures 6e and 6f). As observed for the total and partial mass attenuation coefficients, STH and MER were the soils with the highest values of σ_a and σ_e, in the energy range from 10 to 59.5 keV, while PAR presented the lowest values. The results described show that energies below 30 keV are the best ones to separate soils that present contrasting chemical and physical properties. A good agreement was found between the measured and calculated values of σ_a and σ_e for the [241]Am and ^{137}Cs radioactive sources (Table 4). Relative differences observed between methods were less than 10.5 % (σ_a) and close to 0 % (σ_e). It seems relevant to mention that these two measured parameters plus Z_{eff} and N_{el} were calculated based on the experimental and theoretical values of μ_T and the elemental composition of each soil.

Finally, Z_{eff} and N_{el} demonstrated that the soils were organized in groups according to their compositions (Figures 6g and 6h). Samples from PTB, STH and MER presented the highest Z_{eff} values, which is associated with the amount of Fe_2O_3 measured in these soils (Table 2; Figure 4b). Samples from PGC and MOR were placed in an intermediate position, which is again related to the iron oxide content. The remaining soils were grouped for presenting the lowest Z_{eff} values (Figure 6g). A good agreement was observed between the measured and theoretical values of Z_{eff} and N_{el} for the [241]Am and ^{137}Cs radioactive sources (Table 5). Similar to the results of the other parameters, the relative difference was under 10.5 % (both parameters) found for PGC. As described earlier, Z_{eff} and N_{el} are parameters directly related to the mass attenuation coefficient; thus, the errors mentioned for μ will also influence the results of these two parameters.

Figure 7a shows the PCA graph generated from the results of soil particle size fractions (clay, silt and sand), major oxide (SiO_2, Al_2O_3 and Fe_2O_3) contents, μ_T, μ_{Ph}, μ_{Incoh}, Z_{eff}, N_{el}, σ_a and σ_e totaling 66 variables and ten samples (two principal components PC-1 and PC-2 with a 95.7 % total variance). The axes relate to the loadings, full and broken lines indicate the trends in relation to the variables included in the PCA, that is, percentage of soil fractions, major oxides, and the parameters of nuclear interaction, for each quadrant. The discrimination of the sand soils can be observed in the upper-left quadrant (PAR, JOT and LAP) with the dominance of SiO_2. These samples also presented the highest μ_{Incoh}

Table 4. Atomic (σ_a) and electronic (σ_e) cross-sections of the samples studied for the [241]Am and ^{137}Cs radioactive sources

Sample	σ_a (b per atom)				σ_e (b per electron)			
	59.5 keV		661.6 keV		59.5 keV		661.6 keV	
	Meas.	Th.	Meas.	Th.	Meas.	Th.	Meas.	Th.
PTB	16.511	17.166	2.940	2.890	1.577	1.577	0.259	0.259
PGC	11.488	12.685	2.668	2.736	1.221	1.221	0.258	0.258
STH	17.773	17.796	2.883	2.913	1.621	1.621	0.259	0.259
MER	17.962	17.801	2.939	2.913	1.621	1.621	0.259	0.259
MOR	11.167	12.180	2.722	2.711	1.183	1.183	0.258	0.258
RAZ	9.849	10.128	2.512	2.650	0.997	0.997	0.258	0.258
LAP	9.591	9.979	2.650	2.641	0.985	0.985	0.258	0.258
CAZ	9.480	10.045	2.662	2.647	0.989	0.989	0.258	0.258
JOT	9.419	9.624	2.668	2.632	0.951	0.951	0.258	0.258
PAR	8.810	9.224	2.647	2.607	0.918	0.918	0.258	0.258

Meas. and Th. stand for the measured and theoretical values.

and N_{el} in the following order: PAR > JOT > LAP. Silt (clay loam) and clay samples are mostly located in the lower-left (CAZ, RAZ and MOR) and lower-right (PGC, PTB and MER) quadrants, respectively, mainly influenced by the presence of Al_2O_3 (Figure 7a). The STH soil is located in the upper-right quadrant and MER and PTB are close to this quadrant, which is mainly due to the largest amount of Fe_2O_3 in these soils. The radiation parameters μ_{Ph}, Z_{eff}, σ_a and σ_e are placed in the upper-right quadrant, influenced mainly by the high clay composition of the soils in the following order: STH > MER > PTB (Figure 7a).

The results presented in the PCA (Figure 7a) were confirmed through the dendrogram obtained by the HCA (Figure 7b). The two main clusters observed in the HCA are related

Table 5. Effective atomic number (Z_{eff}) and electron density (N_{el}) of the samples studied for the ^{241}Am and ^{137}Cs radioactive sources

| Sample | Z_{eff} | | | | $N_{el} \times 10^{23}$ (number of electrons g^{-1}) | | | |
| | 59.5 keV | | 661.6 keV | | 59.5 keV | | 661.6 keV | |
	Meas.	Th.	Meas.	Th.	Meas.	Th.	Meas.	Th.
PTB	10.473	10.889	11.351	11.157	2.750	2.859	2.981	2.930
PGC	9.408	10.389	10.321	10.583	2.617	2.889	2.871	2.943
STH	10.967	10.713	11.129	11.245	2.857	2.897	2.899	2.929
MER	11.083	10.984	11.347	11.244	2.888	2.862	2.957	2.930
MOR	9.442	10.299	10.532	10.491	2.664	2.906	2.972	2.960
RAZ	9.878	10.159	9.731	10.263	2.863	2.944	2.820	2.974
LAP	9.734	10.128	10.267	10.230	2.831	2.946	2.987	2.976
CAZ	9.583	10.154	10.312	10.253	2.783	2.949	2.994	2.977
JOT	9.906	10.122	10.338	10.197	2.892	2.955	3.018	2.977
PAR	9.595	10.046	10.259	10.104	2.831	2.964	3.027	2.981

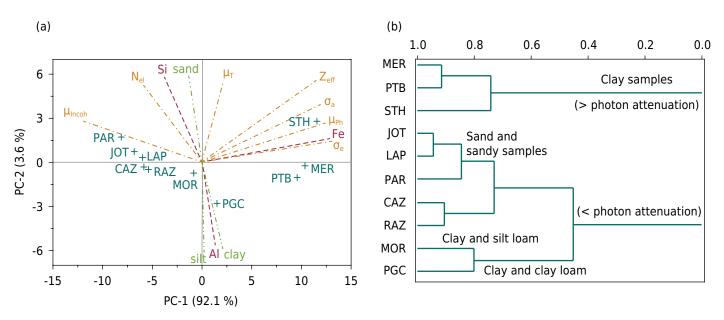Meas. and Th. stand for the measured and theoretical values.

Figure 7. "Scores" of PC-1 and PC-2 of soil samples and their fractions with the inclusion of the following variables: texture (clay, silt and sand percentage), oxide content (SiO_2, Al_2O_3 and Fe_2O_3), total mass attenuation coefficient (μ_T), partial mass attenuation coefficient due to the photoelectric effect (μ_{Ph}), partial mass attenuation coefficient due to the incoherent scattering (μ_{Incoh}), effective atomic number (Z_{eff}), electron density (N_{el}), atomic cross-section (σ_a), and electronic cross-section (σ_e) (a). "Loadings" of the following trends: texture (green lines), oxide content (magenta lines), and radiation interaction with the samples (orange lines). Dendrogram (HCA) for the different soils analyzed with the Euclidian distance, showing the soil samples with the highest and lowest radiation attenuation, influenced mainly by the photoelectric effect and the highest amounts of Fe_2O_3 (b). The acronyms utilized stand for the following municipalities: PTB (Pato Bragado), PGC (Ponta Grossa), STH (Santa Helena), MER (Mercedes), MOR (Morretes), RAZ (Rio Azul), LAP (Lapa), CAZ (Cerro Azul), JOT (Joaquim Távora), and PAR (Paranavaí).

to the soils that had the highest and the lowest radiation attenuation, which allowed the classification of two main clusters with similarities below 0.4. From the soil sample clusters with the highest radiation attenuation, it is possible to highlight the clay soils (MER, PTB and STH) with the highest amounts of Fe_2O_3. Soils from MER and PTB were more similar to each other than STH, which might be associated with differences in the soil mineralogical composition (not investigated in this study) (Figure 7b). As for the soil samples with the lowest radiation attenuation, two clusters can be seen with similarities of 0.5 and 0.7: sandy soils (JOT, LAP and PAR) and clay loam soils (CAZ and RAZ), with predominance of SiO_2; and, clay soils (MOR) and clay loam soils (PGC), the latter presenting the lowest amount of SiO_2 (Table 2; Figure 4b and Figure 7b).

DISCUSSION

When analyzing the radiation interaction with soils, we could observe that the attenuation of the radiation depends on parameters such as the photon energy, chemical composition, and density of the soil. Soils are complex materials composed of variable amounts of clay, silt, and sand as well as oxide contents (Hillel, 2004). These differences indicate that this material has the potential to be used for forensic purposes. The results of our study indicated that the soils studied had textures varying from sand to clay, which influenced their densities and chemical compositions (Tables 1 and 2; Figure 4). We could see that these differences among soils influenced the radiation interaction parameters. Many authors have described the role of the chemical composition of materials in radiation attenuation (Kucuk et al., 2013; Taqi et al., 2016; Ferreira et al., 2018; Camargo et al., 2021; Pires et al., 2021). Recently, Pires et al. (2019) demonstrated the relationship between the soil minerals and radiation interaction parameters, highlighting the particle density importance in the attenuation of the radiation by the matter (Al-Masri et al., 2013). The results of our study reinforce the role of soil composition in photon attenuation, mainly for soils under tropical (PAR and JOT) and subtropical (PTB, PGC, STH, MER, MOR, RAZ, LAP and CAZ) climate.

When radiation interacts with the matter, four processes are considered the most important, namely photoelectric effect, coherent and incoherent scatterings, and pair production (Kaplan, 1963). For low photon energies (<50 keV), the photoelectric effect and the coherent scattering are the dominant processes due to their strong dependence on the atomic number of the constituent elements (Z^{4-5} and Z^{2-3}) (Kucuk et al., 2013; Medhat et al., 2014). With increased photon energy (from 50 to 1 MeV), the incoherent scattering dominates the radiation attenuation by the matter. However, this effect is slightly influenced by the chemical composition of the material due to its linear dependence on Z. When the photon energy reaches 1.022 MeV, the pair production begins to influence the radiation attenuation.

The results obtained demonstrated that for low photon energies (<50 keV), the photoelectric effect was the most important process due to the photon interaction with the bound atomic electrons (Figures 6a and 6b). In addition to the electron binding energies, the atomic number of the atoms present in the soils greatly influences the interaction of the radiation (Kaplan, 1963); helping to explain the differences in the partial attenuation coefficients (μ_{Ph}, μ_{Coh} and μ_{Incoh}) among soils (Figures 6b to 6d). As for the photoelectric effect, the decrease in the photon energy rapidly increases its probability of occurrence, as observed in our results (Murray, 2009; Tarim et al., 2013; Al-Masri et al., 2013; Kucuk et al., 2013; Trunova et al., 2015; Camargo et al., 2021). Regarding the incoherent scattering, which involves the interaction of the photons with the outer and least tightly bound electrons, the low photon energies also presented promising results for soil discrimination. However, the differences in μ_{Incoh} were constant among soils due to the fact that its probability of interaction is nearly independent of the atomic number of the

materials studied (Mudahar et al., 1991; Murray, 2009; Pires et al., 2014; Elmahroug et al., 2015; Ferreira et al., 2018) (Figure 6d).

The mass attenuation coefficient (partial and total) results (energy range from 10 to 59.5 keV) highlighted that the Fe_2O_3 oxide is the most important contributor to the radiation attenuation by the photoelectric effect process in PTB, STH and MER (Table 2; Figures 4b and 6b). On the other hand, the decrease in this oxide content, followed by increased SiO_2 and Al_2O_3 contributions, seems to increase the influence of μ_{Incoh} to μ_T, as observed in PAR (Figure 6d). This is mainly related to the interaction probability dependence of the incoherent scattering on the electron density (Kaplan, 1963; Akkurt et al., 2005; Elmahroug et al., 2015; Prandel et al., 2021).

The electronic cross-section and effective atomic number results indicated that these two parameters could be useful in analyzing radiation interaction for forensic purposes in the soils studied, mainly for low photon energies (Figures 5a and 5b). As described in Ferreira et al. (2018), Z_{eff} depends not only on the atomic number of the soil constituents but also on the number of elements found in the soil, which indicates the importance of differences in soil composition in Z_{eff} (Özdemir and Kurudirek, 2009). This parameter was introduced in nuclear science to describe the properties of composite materials based on their equivalent elements. It is closely related to the electron density of the atoms that make up the soil, which highlights its use to compare soils (Manohara et al., 2008). As for the low photon energies, the photoelectric effect is the main photon interaction process, which is greatly dependent on the atomic number of the soil materials. The highest contribution of this process to μ_T helps to explain the results of Z_{eff} observed among soils (Han and Demir, 2009; Kucuk et al., 2013). For the electronic cross-section, the differences observed in the mass attenuation coefficient help to explain its variation among soils (Table 3). As shown in equation 3, σ_e is approximately proportional to the mass attenuation coefficient (Medhat et al., 2014).

The SiO_2 oxide contents (Table 2; Figure 4b) in the sand soils (Table 1; Figure 4a) influenced the μ_{Incoh} and N_{el} parameters, as noticed in the PCA analysis. This result can be justified by the fact that the incoherent scattering commonly occurs with electrons weakly linked to the atomic nucleus, and this effect is closely related to the number of electrons per gram of sample (Lowenthal and Airey, 2001). Thus, this type of effect is mainly affected by soils when the SiO_2 is the most predominant oxide. On the other hand, μ_{Ph}, Z_{eff}, σ_a and σ_e were mainly influenced by the highest amounts of Fe_2O_3 compared to the amounts of SiO_2 and Al_2O_3 oxide contents found in the soils (Figures 7a and 7b). This is mainly related to the atomic number of iron and its role in the total and partial mass attenuation coefficients due to the photoelectric effect of low-energy photons (few keV). As previously discussed, the photoelectric effect has a Z^{4-5} probability of occurrence, which is greater when the electron is more tightly bound (Kaplan, 1963).

Finally, based on the results presented, we noticed that the PCA and HCA analyses were useful tools to discriminate and find similarities among soils of different regions and characteristics, showing the potential of the methodology presented in this study for forensic purposes.

CONCLUSIONS

The computer-simulation-based method of radiation interaction parameters is a potential tool for forensic soil analysis. Parameters such as mass attenuation coefficient, atomic and electronic cross-sections, effective atomic number, and electron density allowed better discrimination of the soils studied. The data obtained suggested that the lowest photon energies were the best to differentiate the soils, even for those with similar properties like clay, silt, sand, and oxide contents. Multivariate analysis was employed to demonstrate the influence of different soil oxide contents in the radiation attenuation.

Iron oxide significantly influenced the total and partial (photoelectric effect) attenuation coefficients. The lowest photon energies were the most promising ones to discriminate soils based on the influence of the photoelectric effect and the coherent scattering in the mass attenuation coefficient, while for the intermediate photon energies, the incoherent scattering was the most interesting effect. However, photon energies over 59.5 keV practically resulted in no differences among the soil radiation interaction parameters evaluated. Finally, the results of this study also indicated the possible use of radiation interaction parameters for a detailed characterization of soils aiming to support crime scene investigators. The method's main advantage is that it is fast, easy to implement, does not require powerful computers, and the XCOM computer-code can be run online at the NIST website.

ACKNOWLEDGMENTS

AUTHOR CONTRIBUTIONS

Conceptualization: Luiz Fernando Pires (lead).

Formal analysis: Luiz Fernando Pires (equal) and Luis Valério Prandel (equal).

Funding acquisition: Luiz Fernando Pires (lead), Sérgio da Costa Saab (equal) and André Maurício Brinatti (equal).

Methodology: Luiz Fernando Pires (equal) and Luis Valério Prandel (equal).

Writing – original draft: Luiz Fernando Pires (lead), Luis Valério Prandel (equal), Sérgio da Costa Saab (equal) and André Maurício Brinatti (equal).

REFERENCES

Almeida Junior TA, Nogueira MS, Vivolo V, Potiens MPA, Campos LL. Mass attenuation coefficients of X-rays in different barite concrete used in radiation protection as shielding against ionizing radiation. Radiat Phys Chem. 2017;140:349-54. https://doi.org/10.1016/j.radphyschem.2017.02.054

Akkurt I. Determination of effective atomic number and electron density of chitin by gamma-ray attenuation. Int J Phys Sci. 2011;6:5048-50. https://doi.org/10.5897/IJPS11.1211

Akkurt I, Mavi B, Akkurt A, Basyigit C, Kilincarslan S, Yalim HA. Study on Z dependence of partial and total mass attenuation coefficients. J Quant Spectrosc RA. 2005;94:379-85. https://doi.org/10.1016/j.jqsrt.2004.09.024

Al-Masri MS, Hasan M, Al-Hamwi A, Amin Y, Doubal AW. Mass attenuation coefficients of soil and sediment samples using gamma energies from 46.5 to 1332 keV. J Environ Radioact. 2013;116:28-33. https://doi.org/10.1016/j.jenvrad.2012.09.008

Berger MJ, Hubbel JH. XCOM: Photon cross sections on a personal computer. Gaithersburg: National Bureau of Standards; 1987. https://doi.org/10.2172/6016002

Bergslien ET. X-ray diffraction and field portable X-ray fluorescence analysis and screening of soils: project design. Geol Soc. 2013;384:27-46. https://doi.org/10.1144/SP384.14

Blake GR, Hartge KH. Particle density. In: Klute A, editor. Methods of soil analysis: Part 1 Physical and mineralogical methods. Madison: SSSA; 1986. p. 377-82.

Bonetti J, Quarino L. Comparative forensic soil analysis of New Jersey State Parks using a combination of simple techniques with multivariate statistics. J Forensic Sci. 2014;59:627-36. https://doi.org/10.1111/1556-4029.12375

Camargo MA, Kodum KS, Pires LF. How does the soil chemical composition affect the mass attenuation coefficient? A study using computer simulation to understand the radiation-soil interaction processes. Braz J Phys. 2021;51:1775-83. https://doi.org/10.1007/s13538-021-00971-y

Cesareo R, Assis JT, Crestana S. Attenuation coefficients and tomographic measurements for soil in the energy range l0-300 keV. Appl Radiat Isot. 1994;45:613-20. https://doi.org/10.1016/0969-8043(94)90205-4

Cheshire K, Morgan RM, Holmes J. The potential for geochemical discrimination of single- and mixed-source soil samples from close proximity urban parkland locations. Aust J Forensic Sci. 2017;49:161-74. https://doi.org/10.1080/00450618.2016.1144789

Elmahroug Y, Tellili B, Souga C. Determination of total mass attenuation coefficients, effective atomic numbers and electron densities for different shielding materials. Ann Nucl Energy. 2015;75:268-74. https://doi.org/10.1016/j.anucene.2014.08.015

Ferreira TR, Pires LF, Brinatti AM, Auler AC. Surface liming effects on soil radiation attenuation properties. J Soils Sediments. 2018;18:1641-53. https://doi.org/10.1007/s11368-017-1866-2

Gee GW, Bauder JW. Particle-size analysis. In: Klute A, editor. Methods of soil analysis: Part 1 Physical and mineralogical methods. Madison: SSSA; 1986. p. 383-411.

Gonçalves D, Leite WC, Brinatti AM, Saab SC, Iarosz KC, Mascarenhas YP, Carneiro PIB, Rosa JA. Mineralogia de um Latossolo Vermelho distrófico submetido a diferentes manejos por 24 anos. Rev Bras Cienc Solo. 2008;32:2647-52. https://doi.org/10.1590/S0100-06832008000700006

Han I, Demir L. Studies on effective atomic numbers, electron densities and mass attenuation coefficients in Au alloys. J X-Ray Sci Technol. 2010;18:39-46. https://doi.org/10.3233/XST-2010-0238

Han I, Demir L. Determination of mass attenuation coefficients, effective atomic and electron numbers for Cr, Fe and Ni alloys at different energies. Nucl Instrum Methods Phys Res B. 2009;267:3-8. https://doi.org/10.1016/j.nimb.2008.10.004

Hillel D. Introduction to environmental soil physics. San Diego: Elsevier Academic Press; 2004.

Kammrath BW, Koutrakos A, Castillo J, Langley C, Huck-Jones D. Morphologically-directed Raman spectroscopy for forensic soil analysis. Forensic Sci Int. 2018;285:e25-33. https://doi.org/10.1016/j.forsciint.2017.12.034

Kaplan I. Nuclear physics. 2nd ed. Vancouver: Addison-Wesley; 1963.

Kikkawa HS, Naganuma K, Kumisaka K, Sugita R. Semi-automated scanning electron microscopy energy dispersive X-ray spectrometry forensic analysis of soil samples. Forensic Sci Int. 2019;305:109947. https://doi.org/10.1016/j.forsciint.2019.109947

Kucuk N, Tumsavas Z, Cakir M. Determining photon energy absorption parameters for different soil samples. J Radiat Res. 2013;54:578-86. https://doi.org/10.1093/jrr/rrs109

Lal R, Shukla MK. Principles of soil physics. New York: Marcel Dekker; 2004.

Lowenthal GC, Airey PL. Practical applications of radioactivity and nuclear radiations. Cambridge: Cambridge University Press; 2001.

Luo X, Wells LG. Evaluation of gamma ray attenuation for measuring soil bulk density. Part I. Laboratory investigation. Trans ASAE. 1992;35:17-26. https://doi.org/10.13031/2013.28564

Mann KS, Heer MS, Rani A. Effect of low-Z absorber's thickness on gamma-ray shielding parameters. Nucl Instrum Methods Phys Res A. 2015;797:19-28. https://doi.org/10.1016/j.nima.2015.06.013

Manohara SR, Hanagodimath SM, Thind KS, Gerward L. On the effective atomic number and electron density: a comprehensive set of formulas for all types of materials and energies above 1 keV. Nucl Instrum Methods Phys Res B. 2008;266:3906-12. https://doi.org/10.1016/j.nimb.2008.06.034

Medhat ME, Pires LF. Importance of photo atomic cross section for studying physical properties of different types of soil. X-Ray Spectrom. 2016;45:202-06. https://doi.org/10.1002/xrs.2689

Medhat ME, Pires LF, Arthur RCJ. Analysis of photon interaction parameters as function of soil composition. J Radioanal Nucl Ch. 2014;300:1105-12. https://doi.org/10.1007/s10967-014-3028-y

Melo VF, Testoni SA, Dawson LA, Salvador FAS. Sand fraction is not suitable for forensic investigations in subtropical soils. Rev Bras Cienc Solo. 2020;44:e0190174. https://doi.org/10.36783/18069657rbcs20190174

Mudahar GS, Modi S, Singh M. Total and partial mass attenuation coefficients of soil as a function of chemical composition. Int J Radiat Appl Instr A. 1991;42:13-8. https://doi.org/10.1016/0883-2889(91)90118-K

Murray R. Nuclear energy: An introduction to the concepts, systems, and applications of nuclear processes. 6th ed. Burlington: Butterworth-Heinemann; 2009.

Nakai I, Furuya S, Bong W, Abe Y, Osaka K, Matsumoto T, Itou M, Ohta A, Ninomiya T. Quantitative analysis of heavy elements and semi-quantitative evaluation of heavy mineral compositions of sediments in Japan for construction of a forensic soil database using synchrotron radiation X-ray analyses. X-ray Spectrom. 2013;43:38-48. https://doi.org/10.1002/xrs.2486

National Institute of Standards and Technology - NIST. XCOM: Photon cross sections database - NIST Standard Reference Database 8 (XGAM) [internet]. Gaithersburg: NIST; 2016 [cited 22 June 2016]. Available from: https://www.nist.gov/pml/xcom-photon-cross-sections-database

Özdemir Y, Kurudirek MA. Study of total mass attenuation coefficients, effective atomic numbers and electron densities for various organic and inorganic compounds at 59.54 keV. Ann Nucl Energy. 2009;36:1769-73. https://doi.org/10.1016/j.anucene.2009.09.008

Pires LF. Soil analysis using nuclear techniques: A literature review of the gamma ray attenuation method. Soil Till Res. 2018;184:216-34. https://doi.org/10.1016/j.still.2018.07.015

Pires LF, Brinatti AM, Prandel LV, Saab SC. Mineralogical composition of hardsetting soils and its effect on the radiation attenuation characteristics. J Soils Sediments. 2016;16:1059-68. https://doi.org/10.1007/s11368-015-1318-9

Pires LF, Cássaro FAM, Correchel V. The use of nuclear techniques in soil science: a literature review of the Brazilian contribution. Rev Bras Cienc Solo. 2021;45:e0210089. https://doi.org/10.36783/18069657rbcs20210089

Pires LF, Leite WC, Brinatti AM, Saab SC. Radiation attenuation properties based on the quantification of soil components using the Rietveld Method. Results Phys. 2019;12:2009-11. https://doi.org/10.1016/j.rinp.2019.02.036

Pires LF, Prandel LV, Saab SC. The effect of wetting and drying cycles on soil chemical composition and their impact on bulk density evaluation: an analysis by using XCOM data and gamma-ray computed tomography. Geoderma 2014;213:512-20. https://doi.org/10.1016/j.geoderma.2013.09.003

Prandel LV, Dias NMP, Saab SC, Brinatti AM, Giarola NFB, Pires LF. Characterization of kaolinite in the hardsetting clay fraction using atomic force microscopy, X-ray diffraction, and the Rietveld method. J Soils Sediments. 2017;17:2144-55. https://doi.org/10.1007/s11368-017-1654-z

Prandel LV, Melo VF, Brinatti AM, Saab SC, Salvador FAS. X-ray diffraction and Rietveld refinement in Deferrified clays for forensic science. J Forensic Sci. 2018;63:251-7. https://doi.org/10.1111/1556-4029.13476

Prandel LV, Melo VF, Testoni SA, Brinatti AM, Saab SC, Dwason LA. Spectroscopic techniques applied to discriminate soils for forensic purposes. Soil Res. 2019;58:151-60. https://doi.org/10.1071/SR19066

Prandel LV, Saab SC, Tonial LMS, Brinatti AM, Pires LF. Can the granulometric soil fractions attenuate the radiation differently from the whole soil? Braz Arch Biol Technol. 2021;64:e21190760. https://doi.org/10.1590/1678-4324-2021190760

Sposito G. The Chemistry of Soils. 2nd ed. Oxford: Oxford University Press; 2008.

Tanner CB, Jackson ML. Nomographs of sedimentation times for soil particles under gravity or centrifugal acceleration. Soil Sci Soc Am Proc. 1948;12:60-5. https://doi.org/10.2136/sssaj1948.036159950012000C0014x

Taqi AH, Al Nuaimy QAM, Karem GA. Study of the properties of soil in Kirkuk, IRAQ. J Radiat Res Appl Sci. 2016;9:259-65. https://doi.org/10.1016/j.jrras.2016.02.006

Taqi AH, Ghalib AM, Mohammed HM. Shielding properties of Cu-Sn-Pb alloy by Geant4, XCOM and experimental data. Mater Today Commun. 2021;26:101996. https://doi.org/10.1016/j.mtcomm.2020.101996

Tarim UA, Gurler O, Ozmutlu EN, Yalcin S. Monte Carlo calculations for gamma-ray mass attenuation coefficients of some soil samples. Ann Nucl Energy. 2013;58:198-201. https://doi.org/10.1016/j.anucene.2013.03.021

Testoni SA, Melo VF, Dawson LA, Salvador FAZ, Kunii PA. Validation of a standard operating procedure (SOP) for forensic soils investigation in Brazil. Rev Bras Cienc Solo. 2019;43:e0190010. https://doi.org/10.1590/18069657rbcs20190010

Testoni AS, Melo VF, Dawson LA, Salvador FAZ, Prandel LV. Evaluation of forensic soil traces from a crime scene: robbery of a safety deposit box in Brazil. Geol Soc. 2020;492:181-96. https://doi.org/10.1144/SP492-2019-35

Trunova V, Sidorina A, Kriventsov V. Measurement of X-ray mass attenuation coefficients in biological and geological samples in the energy range of 7–12keV. Appl Radiat Isot. 2015;95:48-52. https://doi.org/10.1016/j.apradiso.2014.09.017

Uitdehaag S, Wiarda W, Donders T, Kuiper I. Forensic comparison of soil samples using nondestructive elemental analysis. J Forensic Sci. 2017;62:861-8. https://doi.org/10.1111/1556-4029.13313

United States Department of Agriculture. Soil mechanics: USDA textural soil classification. Study guide. Washington, DC: United States Department of Agriculture; 1987.

Woods B, Kirkbride KP, Lennard C, Robertson J. Soil examination for a forensic trace evidence laboratory – Part 2: Elemental analysis. Forensic Sci Int. 2014;245:195-201. https://doi.org/10.1016/j.forsciint.2014.10.018